Dramatic Improvement of Parallel Imaging with High Dielectric Material – Demonstration with Electromagnetic Field Calculations at 123 MHz

Zhipeng Cao[1], Wei Luo[1], Christopher T. Sica[1], Sukhoon Oh[2], Sebastian Rupprecht[1], Giuseppe Carluccio[2], Christopher M. Collins[2], and Qing X. Yang[1]
[1]*Radiology, The Pennsylvania State University, Hershey, PA, United States,* [2]*Radiology, New York University, New York City, NY, United States*

Introduction: Utilization of low loss high dielectric material (HDM) has been reported with improved efficiency in both transmit and receive RF fields at 3 T and 7 T [1-5]. These initial studies revealed that, in addition to the overall RF field enhancement, the distributions of the field were significantly altered with greater intensity focused in the regions near the HDM [1, 2]. These novel enhancements of RF field are desirable for improvement of parallel imaging [6, 7], especially, for the cases with higher levels of data under-sampling. A theoretical study is thus presented here on potential utilization of HDM for parallel imaging at 3 T with computer modeling of a standard configuration including a body volume coil for transmission and multichannel head array for reception. It is demonstrated that incorporation of HDM into RF coils dramatically improved transmission efficiency of the body coil, head array receive efficiency and spatial characteristics of SENSE *g*-factor.

Method: In order to examine the influence of HDM on parallel imaging, the transmit power efficiency of the body coil, noise correlation matrix and receive signal-to-noise (SNR) efficiency of the receive array (without any k-space data undersampling), and SENSE *g*-factor (with data undersampling accelerations x2, x3, and x4) were all calculated and evaluated in cases without and with HDM. The configuration of coils, phantom, and HDM are shown in Fig.1. The cylindrical phantom was modeled with conductivity = 0.5 S/m, relative permittivity = 55, length = 300 mm, and radius = 60 mm. HDM was modeled with conductivity = 0.01 S/m, relative permittivity = 1100, length = 60 mm, inner radius = 60 mm, outer radius = 80 mm. The permittivity of the HDM was determined after a parameter sweep of the relative permittivity within 500~2500, and it was found that a relative permittivity of 1100 yields the optimal transmission efficiency for the body coil with the phantom. The electromagnetic field calculations were performed using XF7 (Remcom Inc.) with 4 mm grid resolution. The transmit coil efficiency is calculated as $B_1^+/\sqrt{P}$, where B_1^+ is the transmit rotating magnetic field, P the power dissipated in the phantom and HDM. The receive SNR efficiency is defined here as $\sqrt{B_1^{-H} * R^{-1} * B_1^-}$ based on published method [8], where B_1^- is the multichannel receive rotating magnetic field matrix. The 8x8 noise matrix R is calculated as $R_{ij} = \Delta x \Delta y \Delta z \sum_k (\sigma_k E_{ki} \cdot E_{kj}^*)$ for the 8-element receive array, where E_{ki} is the electric field of voxel k from channel i, Δx, Δy, and Δz the voxel size in x, y, and z directions. The SENSE *g*-factor is calculated following standard definition [6].

Results: As shown in Fig. 2, improvement in transmit efficiency of the body coil is achieved with HDM: from 2-fold at center up to 5-fold at periphery, which predicts a several fold reduction of RF excitation power for the given sample. The ratio of array receive efficiency with and without HDM exhibits a similar trend with improvement from 10% at center up to 250% at periphery, indicating that when full data sampling is used, placement of HDM can dramatically improve receive efficiency at phantom periphery with no degradation at center. The noise correlation matrices for the receive array in Fig. 3 show that the HDM increased the noise correlation among adjacent channels, but decreased the correlation among distant channels. Since the inverse *g*-factor maps shown in Fig. 4 is proportional to image SNR, they indicate that the SNR can be significantly improved with HDM. Specifically, the inverse *g*-factor value at the center is more than doubled with x4 reduction. Notice that the head array model has more overlaps between adjacent channels than a standard array and resulted in large values of off-diagonal elements in the noise matrix (Fig. 3 (left), which highlighted the effects of HDM on the parallel imaging parameters.

Discussions: The relative permittivity 1100 used in this computer modeling study was much higher than previous studies. Dielectric materials with relative permittivity in this range have been used broadly and are available for MRI applications. Although the transmit magnetic field inhomogeneities with the presence of the HDM may pose challenges for some applications, and advanced pulsing strategies for homogenizing the field may need to be developed for these cases, the receive efficiency analyzed here should still be valid. Further investigations are being performed with different sample sizes and main magnetic field strengths, and with arrays with varying number of channels.

Conclusions: Utilization of HDM with very high permittivity and minimal conductivity can potentially achieve several fold improvement of RF transmission and reception efficiencies with standard hardware. Particularly, the improvement of receive arrays will lead to improved image SNR with various levels of data undersampling. These findings will serve as general direction and guidance for more sophisticated design and placement of HDM in practice.

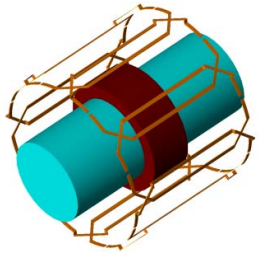

FIG. 1. Simulation setup of phantom (blue), HDM (dark red), and receive head array, inside a transmit body coil (not shown).

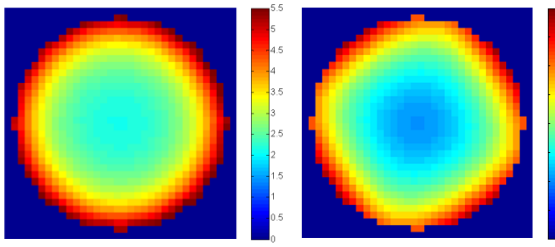

FIG. 2. Transmit body coil (left) and receive head array (right) efficiency improvements in phantom (with HDM divided by without).

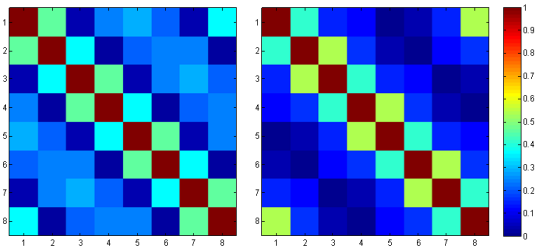

FIG. 3. Noise correlation matrices of the receive array and phantom without (left) and with (right) HDM.

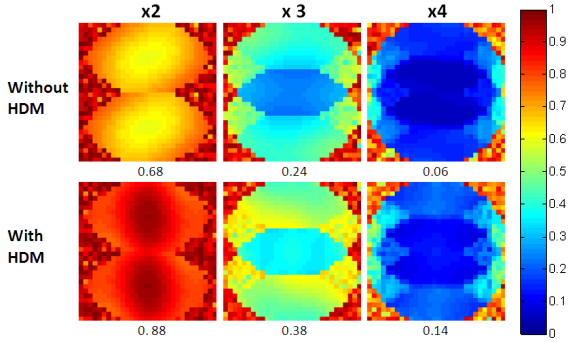

FIG. 4. Maps of inverse *g*-factor (*1/g*) at various one-dimensional accelerations (x2, x3, and x4) for the 8-channel array setup (Fig.1) without (top row) and with (bottom row) HDM. Center *1/g* values are shown below each map.

References: **[1]** Yang *et al.*, JMRI 2006; 24: 197–202. **[2]** Yang *et al.*, MRM 2010; 65: 358–362. **[3]** Teeuwisse *et al.*, MRM 2011; 67: 1285–1293. **[4]** Teeuwisse *et al.*, MRM 2012; 67: 912–918. **[5]** Luo *et al.*, MRM 2012, *in press*. **[6]** Pruessmann *et al.*, MRM 1999; 42: 952–962. **[7]** Griswold *et al.*, MRM 2002; 47: 1202–1210. **[8]** Kellman & McVeigh, MRM 2005; 54: 1439–1447.
Acknowledgement: Funding through NIH R01 EB000454.